Effect of Grain Refinement on Electrochemical Behavior of Al–Zn–Mg–Cu Alloys

Qingqing Sun[1,2,3], Kanghua Chen[2,], Huachan Fang[2], Jie Xu[2], Pengxuan Dong[2], Guiyun Hu[2], Qiyuan Chen[1,*]*

[1] School of Chemistry and Chemical Engineering, Central South University, Changsha 410083, Hunan, China
[2] State Key Laboratory of Powder Metallurgy, Central South University, Changsha 410083, Hunan, China
[3] School of Chemical Engineering, Purdue University, West Lafayette 47907, IN, USA
[*]E-mail: khchen@csu.edu.cn, cqy@csu.edu.cn

The influence of Yb, Cr and Zr additives on electrochemical corrosion and stress cracking corrosion behavior of Al–6.2Zn–2.3Mg–2.3Cu (mass fraction) alloys was investigated using open circuit potential, electrochemical impedance spectroscopy, cyclic polarization and U-type method. Better corrosion resistance of Al alloys was obtained through grain refinement effect by adding 0.16Zr and 0.16Zr–0.18Cr–0.3Yb. Both strength and corrosion resistance are inversely proportional to grain size, showing a Hall-Petch relation. The mechanism of grain refinement effect was revealed by TEM.

1. INTRODUCTION

Al alloys have been successfully used as the primary material for aircraft industry for more than 80 years. The 7000 series of Al alloys show higher strength compared to other classes of Al alloys and are selected in the fabrication of upper wing skins, stringers and horizontal/vertical stabilizers [1, 2]. However, due to their compositions, one limitation of their use is the low resistance to corrosion, e.g., pitting corrosion [3, 4], inter-granular corrosion (IGC) , exfoliation corrosion [5] and stress cracking corrosion (SCC) [6].

In order to improve corrosion resistance of 7000 series Al alloys, the design and control of chemical composition and the development of more effective heat treatments are desirable [1, 7]. In

recent years, researchers showed great interests on micro-alloying additions such as Zr [8], Cr [9], and Sc [10, 11] due to these additives could reduce recrystallization degree by forming new dispersoids, thus producing more of low angle grain boundaries (LAGB). Compared with High angle grain boundaries (HAGB), LAGB are less vulnerable to localized corrosion. Therefore, the corrosion resistance of 7000 series alloys might be greatly improved by grain refinement which is caused by the inhibiting of recrystallization. N. Birbilis and his coworkers [9, 12, 13] reviewed that there is a tendency for corrosion rate to decline as grain size decreases in many alloy systems.

Zr additions have been used widely in commercial 7000 series Al alloys due to the formation of Al_3Zr dispersoids, but the recrystallization of alloys cannot be impeded completely by it [14]. Further adding Cr to Al–Zr alloys could form more thermally stable $L1_2$ structural $Al_{69}Cr_6Zr$ dispersoids, providing higher strength compared to Al_3Zr dispersoids [15]. Addition of Sc to Al–Zn–Mg–Cu alloys can produce Al_3Sc dispersoids which are more effective than Al_3Zr dispersoids, thus effectively inhibit recrystallization and enhance the SCC resistance [16]. Finer and more stable $Al_3(Sc, Zr)$ dispersoids are formed by complex additions of Sc and Zr, as a result, reducing the degree of recrystallization more effectively [17, 18]. However, Sc is too expensive for the commercial application of Sc-containing Al–Zn–Mg–Cu alloys. Cheaper rare earth (RE) alloys like Y [19], Er [20, 21], Ce [16, 22] and Yb [23, 24] could be alternatives. Similarly to $Al_3(Sc, Zr)$ dispersoid, thermally stable $Al_3(Sc, RE)$ dispersoids formed and lead to the improvement of strength properties as well as corrosion resistance.

In previous work [15, 20, 24-29], we studied the effect of Yb, Cr and Zr additives on microstructures and properties of T6 aged Al–Zn–Mg–Cu alloys with high zinc (8.6 wt%). T6 aged alloy usually is susceptible to localized corrosion and stress cracking corrosion. High zinc provides a high strength but leads to the decline of corrosion resistance. For the further improvement of corrosion resistance, in the present work, retrogression and re-ageing (RRA) T77 aged low zinc alloy (Al–6.2Zn–2.3Mg–2.3Cu) was selected as the base alloy. The effects of Yb, Cr and Zr additions on microstructure, strength and corrosion properties of base alloy were systematically investigated.

2. EXPERIMENTAL

2.1 Materials and processing

The compositions of the three studied alloys are shown in Table 1. High purity aluminum (99.9%), zinc (99.9%) and magnesium (99%), and Al–Cu, Al–Zr, Al–Cr and Al–Yb master alloys were smelted at the temperature of 700–740 ^{0}C. The alloys melt were refined by adding 0.2–0.4 wt% C_2Cl_6, and then cast into Ø 45 mm ingots in iron mould. The ingots were treated at 460 ^{0}C for homogenization for 24 h, followed by extrusion at the temperature of 410–430 ^{0}C into plate of 16 mm × 11 mm section with 9 extrusion ratio. The extruded plates were held at 480 ^{0}C for 1 h for solution treatment, followed by water quench to room temperature. Then the plates were aged with RRA T77 temper (120 ^{0}C × 24h + 180 ^{0}C × 0.5h + 120 ^{0}C × 24h).

Table 1. Composition of the studied Al–Zn–Mg–Cu alloys (mass fraction)

Alloys	Zn	Mg	Cu	Zr	Cr	Yb	Al
AlZnMgCu	6.2	2.3	2.3	/	/	/	Bal.
AlZnMgCu–Zr	6.2	2.3	2.3	0.16	/	/	Bal.
AlZnMgCu–Zr–Cr–Yb	6.2	2.3	2.3	0.16	0.18	0.3	Bal.

2.2 Microstructure

Microstructure characterization was performed with optical microscopy (OM) and transmission electron microscopy (TEM). The samples for OM were prepared by Graff-Sargent reagent.

2.3 Hardness

Vickers hardness was measured by loading 294 N with a HBRUV-187.5 instrument on the surface of T77 aged specimens. Hardness values are the mean values of at least five measurements.

2.4 Stress cracking corrosion

U-type testing was carried out to measure the SCC of the specimens after T77 ageing treatment. The U-type specimen with 522 MPa applied stress is shown in Fig. 1. After being polished and ultrasonically cleaned, the U-type specimens were constantly exposed to 4 mol/L NaCl solution under the temperature of $35\pm1\ ^0C$,until the samples revealed cracks or broken into two pieces.
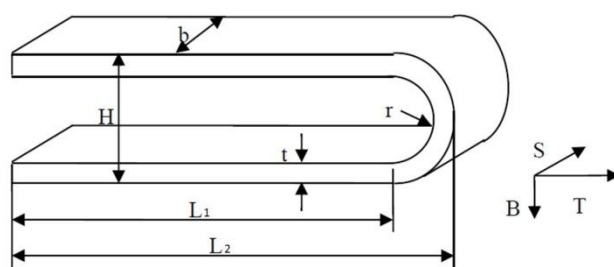

Figure 1. Geometry of U-type specimen

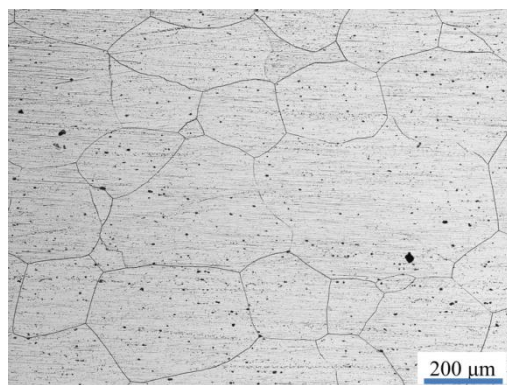*2.5 Electrochemical corrosion*

For electrochemical characterization, T77 aged samples were wet ground through successive grades of silicon carbide abrasive papers from P240 to P1500, followed by diamond finishing to 0.1 μm. A CHI 660C electrochemical workstation (3700 Tennison Hill Drive1 Austin, TX787381, USA) connected to a three-electrode cell was used for the electrochemical measurements. The working electrode was the test material with an immersed area of 0.5 cm^2 and platinum plate and saturated

calomel (SCE) electrodes were used as the counter and reference electrodes, respectively. The test solution for open circuit potential (OCP) and electrochemical impedance spectroscopy (EIS) measurements was 3.5 wt% NaCl. Electrochemical impedance spectroscopy (EIS) measurements were conducted after the OCP was stable. The frequency ranged from 10 kHz to 1 Hz and the amplitude of the sinusoidal potential signal was 10 mV with respect to the OCP. The impedance spectra were analyzed using ZView™ (Scribner Associates Inc.) electrochemical analysis software. Cyclic polarization curves were carried out in two solutions, i.e. 3.5 wt% NaCl and 0.1 mol/L Na_2SO_4 + 10 mmol/L NaCl, at a scanning rate of 1 mV/s, ranging from -1.0 to -0.4 V_{SCE} for 3.5 wt% NaCl solution from -1.0 to -0.2 V_{SCE} for the other. All electrochemical tests were performed under room temperature in a faraday cage. All the electrochemical parameters listed in the present paper are the mean values of at least three tests.
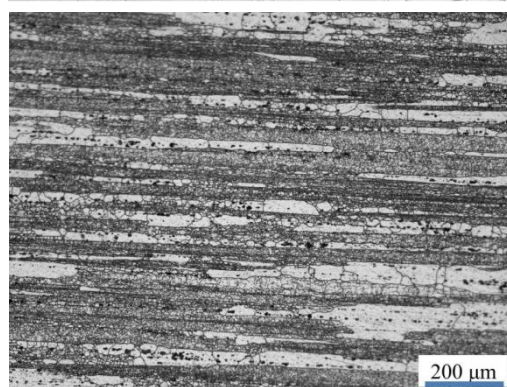
3. RESULTS

3.1 Optical microstructure

The optical microstructures of T77-tempered alloys are shown in Fig. 2. AlZnMgCu alloy is completely recrystallized (Fig. 2a), the mean grain size is as large as ~300 μm. AlZnMgCu–Zr alloy exhibits partially recrystallized microstructure (Fig. 2b) and AlZnMgCu–Zr–Cr–Yb alloy has fibrous unrecrystallized microstructure with fine subgrains (Fig. 2c).
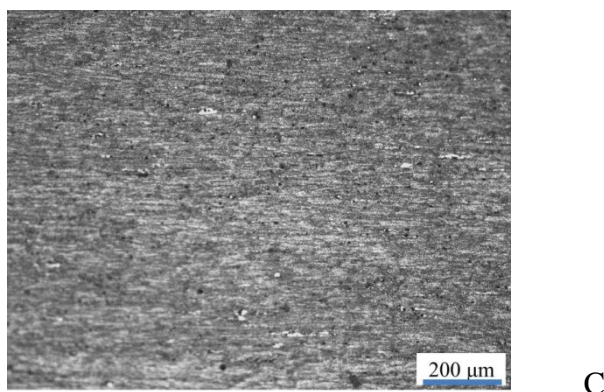

A

B

C

Figure 2. Optical microstructures of Graff-Sargent reagent etched (a) completely recrystallized AlZnMgCu alloy, (b) partially recrystallized AlZnMgCu–Zr alloy and (c) completely unrecrystallized AlZnMgCu–Zr–Cr–Yb alloy.

The grain refinement effect of Al–Zn–Mg–Cu alloy is achieved by Zr, Cr and Yb additions. Only adding Zr cannot completely inhibit recrystallization of Al matrix, while complex additions of Zr, Cr and Yb can more significantly inhibit recrystallization and further refine the grain size.

3.2 Stress cracking corrosion

The effect of micro-alloying additions on the SCC resistance of Al alloys is shown in Table 2. AlZnMgCu U-type specimens break down in less than two days. Compared to AlZnMgCu alloy, the SCC resistance of AlZnMgCu–Zr–Cr–Yb alloy improves dramatically since the U-type specimens don't fail for months. Undoubtedly, this is of great application value for 7000 series Al alloys because they are usually served under huge applied stress. Adding 0.16Zr also can prolong the cracking period but to a relative limited extent. In a word, grain refinement effect can greatly enhance the SCC resistance of the studied alloys. This result is in good agreement with our previous work on Al-8.6Zn-xMg-xCu alloys [24, 25, 27, 28].

Table 2. SCC initiation time of Al alloys with different micro-alloys

Alloy	time /h			Mean time /h
AlZnMgCu	39.5	44	45.5	43
AlZnMgCu–Zr	282	289.5	325	299
AlZnMgCu–Zr–Cr–Yb	619	1536	1680	1278

3.3 OCP

The open circuit potential vs time curves of Al alloys with different micro-alloying additions are determined in 3.5 wt% NaCl solution under room temperature. As presented in Fig. 3, after adding Zr or Zr–Cr–Yb to Al–Zn–Mg–Cu alloy, OCP shifts to more positive (anodic) direction, indicating

less corrosion susceptibility for alloys with micro-alloys. And AlZnMgCu–Zr–Cr–Yb alloy has the least inclination to corrosion in 3.5 wt% NaCl solution.
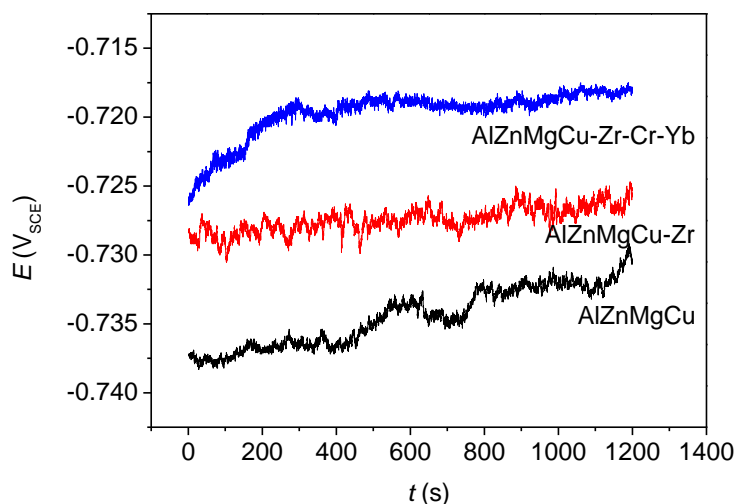

Figure 3. OCP vs time curves of the studied alloys in 3.5 wt% NaCl solution

3.4 EIS

The EIS of the studied alloys in 3.5 wt% NaCl solution is shown in Fig. 4. Though overlapped, two capacitance loops still can be distinguished from Bode plots in Fig. 4c. An equivalent electrical circuits model $R_s(CPE_p(R_{pit}(CPE_{pit} \cdot R_{ct})))$ shown in Fig. 5 is used for quantitative analysis. The physical meaning of the equivalent circuit elements is as follow:

1. R_s,   ohmic resistance of the electrolyte
2. CPE_p,   constant phase element of passive film
3. R_{pit},   film pore resistance
4. CPE_{pit},   constant phase element of the double layer
5. R_{ct},   charge transfer resistance

The element CPE is used to represent the possibility of a non-ideal capacitance. It is commonly used for the surface with uneven current distribution or with increased surface roughness. The impedance of CPE (Z_{CPE}) is related to the angular frequency:

$$Z_{CPE(\omega)} = [Cj\omega^{-n}]^{-1} \quad (1)$$

Where $j^2 = -1$, and n is an empirical exponent varies between 0 and 1. When n = 1, the CPE represents a purely capacitive behavior associated with a perfectly smooth surface; when n = 0, the CPE is a resistor.
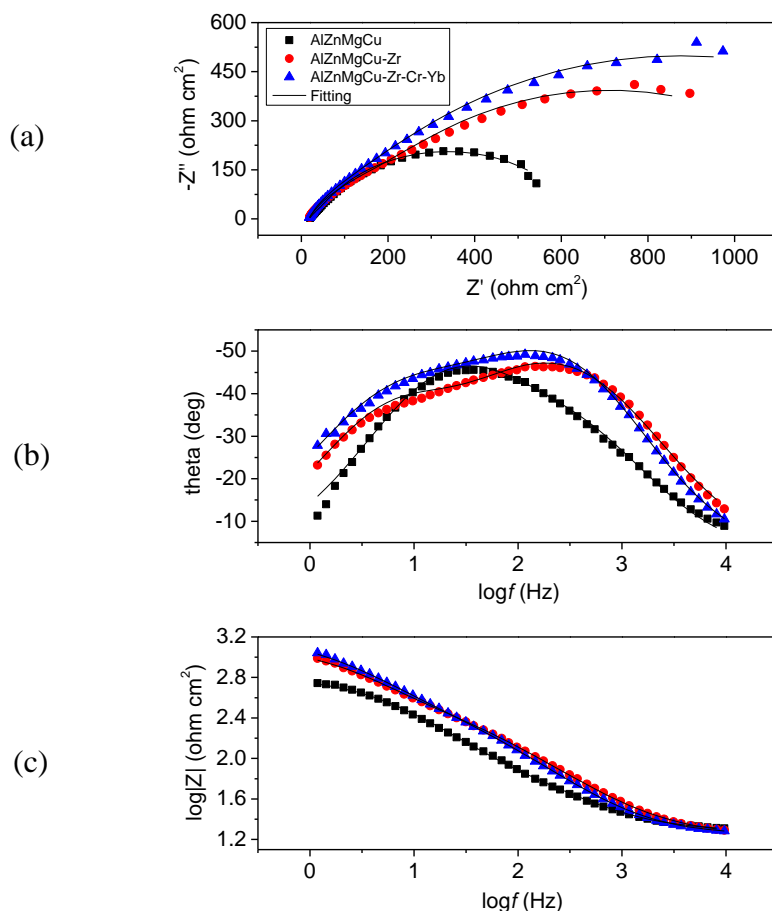
Figure 4 EIS of AlZnMgCu alloy, AlZnMgCu–Zr alloy and AlZnMgCu–Zr–Cr–Yb alloy in 3.5 wt% NaCl solution: (a) Nyquist plots; (b) (c) Bode plots
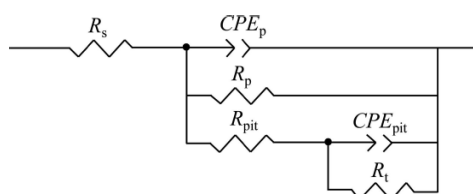

Figure 5. Equivalent circuits of EIS

Table 3. Fitting results of EIS plots

Alloy	R_s $\Omega \cdot cm^2$	Q_p S s^p/cm^2	n_1	R_{pit} $\Omega \cdot cm^2$	Q_{pit} S s^p/cm^2	n_2	R_{ct} $\Omega \cdot cm^2$	$R_p = R_{pit} + R_{ct}$ $\Omega \cdot cm^2$
AlZnMgCu	19.04	8.43×10^{-5}	0.75	103	6.23×10^{-5}	0.77	519	622
AlZnMgCu–Zr	16.97	6.37×10^{-5}	0.73	413	1.02×10^{-4}	0.79	863	1276
AlZnMgCu–Zr–Cr–Yb	17.54	5.41×10^{-5}	0.77	376	1.09×10^{-4}	0.70	1260	1636

The fitting data is shown in Table 3, from which we can know that polarization resistances R_p ($R_p = R_{pit} + R_{ct}$) of AlZnMgCu alloy, AlZnMgCu–Zr alloy and AlZnMgCu–Zr–Cr–Yb alloy is 622 $\Omega \cdot cm^2$, 1276 $\Omega \cdot cm^2$ and 1636 $\Omega \cdot cm^2$, respectively. A larger R_p or R_{ct} value means a greater resistance to corrosion. The EIS results are consistent with OCP results.

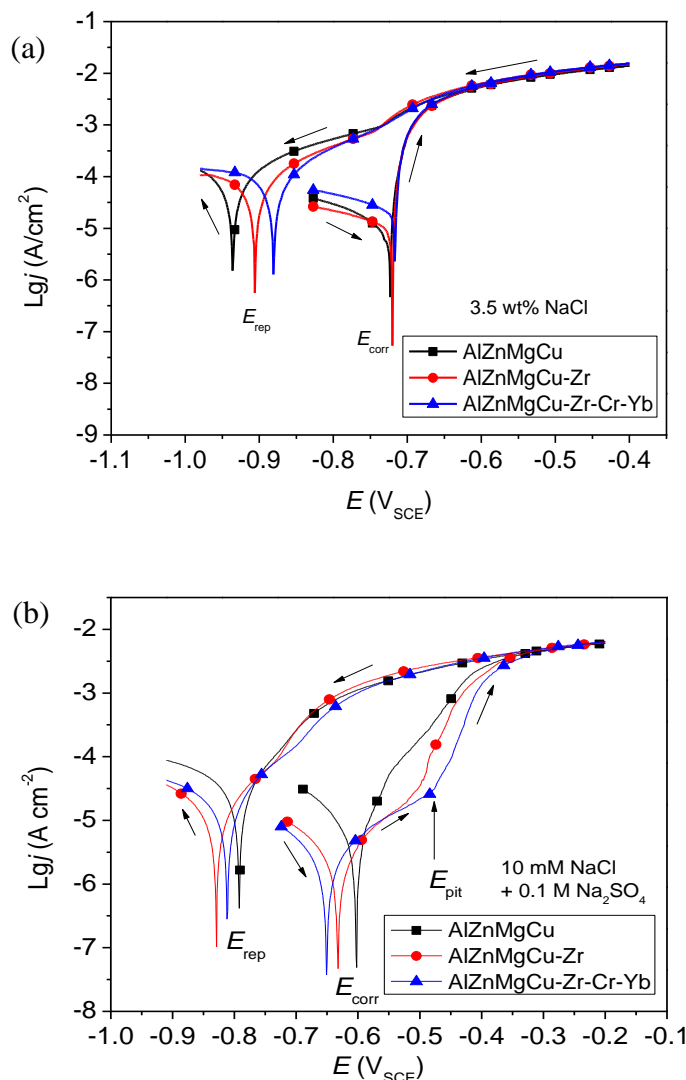*3.5 Cyclic polarization*

Figure 6. Cyclic polarization curves of AlZnMgCu alloy, AlZnMgCu–Zr alloy and AlZnMgCu–Zr–Cr–Yb alloy in (a) 3.5 wt% NaCl solution and in (b) 0.1 mol/L Na_2SO_4 + 10 mmol/L NaCl solution.

Cyclic polarization tests can accelerate the corrosion process and can evaluate the corrosion resistance or degradation rate in a short time. Fig. 6a shows cyclic polarization curves of Al alloys in 3.5 wt% NaCl solution. As can be seen, there is a distinct difference between repassivation potentials of different alloys. However, due to the absent of Tafel zone on the curves, corrosion current densities (J_{corr}), which are used to quantify the corrosion rate, cannot derived from polarization curves. Pitting

potential (E_{pit}), a key parameter which is related to pitting corrosion, also is absence. In order to obtain obvious pitting potentials, a trace chloride-containing solution (0.1 mol/L Na_2SO_4 + 10 mmol/L NaCl) was selected as the electrolyte, and the corresponding cyclic polarization plots are shown in Fig. 6b.

Electrochemical parameters such as corrosion potential (E_{corr}), repassivation potential (E_{rep}), pitting potential (E_{pit}) and corrosion current density (J_{corr}) of alloys in 3.5 wt% NaCl solution and 0.1 mol/L Na_2SO_4 + 10 mmol/L NaCl solution (Trace NaCl) are listed Table 4. J_{corr} represents the corrosion rate of alloys. In trace chloride-containing solution, the measured J_{corr} of AlZnMgCu alloy, AlZnMgCu–Zr alloy and AlZnMgCu–Zr–Cr–Yb alloy is 9.55×10^{-6} A/cm^2, 3.09×10^{-6} A/cm^2 and 1.99×10^{-6} A/cm^2, respectively. This implies a lower corrosion rate for alloys with addition of Zr and Zr–Cr–Yb. The anodic current density limit which corresponds to current density when applied anodic potential is far away from corrosion potential also can be used as corrosion rate criterion. It can be seen in Fig. 6b, at the same anodic potential, the current density limit of AlZnMgCu alloy is the highest, whereas that value of AlZnMgCu–Zr–Cr–Yb alloy is the lowest.

Table 4. Parameters of cyclic polarization curves

Solution	Alloy	J_{corr} A/cm^2	E_{corr} V_{SCE}	E_{pit} V_{SCE}	E_{rep} V_{SCE}
3.5 wt% NaCl	AlZnMgCu	/	-0.723	/	-0.936
	AlZnMgCu–Zr	/	-0.720	/	-0.906
	AlZnMgCu–Zr–Cr–Yb	/	-0.717	/	-0.881
Trace NaCl	AlZnMgCu	9.55×10^{-6}	-0.602	-0.568	-0.792
	AlZnMgCu–Zr	3.09×10^{-6}	-0.632	-0.499	-0.819
	AlZnMgCu–Zr–Cr–Yb	1.99×10^{-6}	-0.650	-0.478	-0.812

E_{corr} is not a thermodynamic parameter and its value is determined by both of the anodic and cathodic branches, so that E_{corr} as the criterion to evaluate corrosion behavior is empirical in nature [30]. As listed in Table 4, in 3.5 wt% NaCl solution, the E_{corr} shifts to the positive (anodic) direction with more additives, which is the opposite with the trend found in the solution of 0.1 mol/L Na_2SO_4 + 10 mmol/L NaCl. Previous studies indicated that, in 3.5 wt% NaCl and more aggressive solutions, E_{corr} shifts to the positive direction with improved corrosion resistance [31-33]; on the contrary, in solution containing trace chloride, E_{corr} shifts to the negative direction with improved corrosion performance . Therefore, based on the E_{corr} data obtained from both 3.5 wt% NaCl solution and 0.1 mol/L Na_2SO_4 + 10 mmol/L NaCl, we can conclude that enhanced corrosion resistance is achieved by further grain refinement.

E_{pit} is one of the most valuable parameters to evaluate pitting corrosion behavior. However, in some media it only appears at a relative low scan rate (e.g. less than 0.1 mv/s in 3.5 wt% NaCl), implying that a very long testing time is needed. Even E_{pit} can be obtained in 3.5 wt% NaCl, the potential gap of the studied alloys is usually small and undistinguishable. In order to enlarge the pitting potential gaps, we chose a solution containing trace chloride ions (0.1 mol/L Na_2SO_4 + 10 mmol/L NaCl) as electrolyte for tafel tests. The pitting potential of AlZnMgCu alloy, AlZnMgCu–Zr alloy and

AlZnMgCu–Zr–Cr–Yb alloy is -0.568, -0.499 and -0.478 V_{SCE}, respectively, indicating that the resistance to pitting corrosion of the alloys can be substantially improved by adding micro-alloys like Zr, Cr and Yb.

4. DISCUSSION

4.1 Consistence of SCC result and potential differences

The SCC results and electrochemical results show excellent agreement with each other, as shown in Fig. 7. With different micro-alloying additions, the value of SCC initiation time shows the same trend with E_{pit}, E_{pit}–E_{corr}, E_{pit}–E_{rep} as well as E_{rep}–E_{corr}.
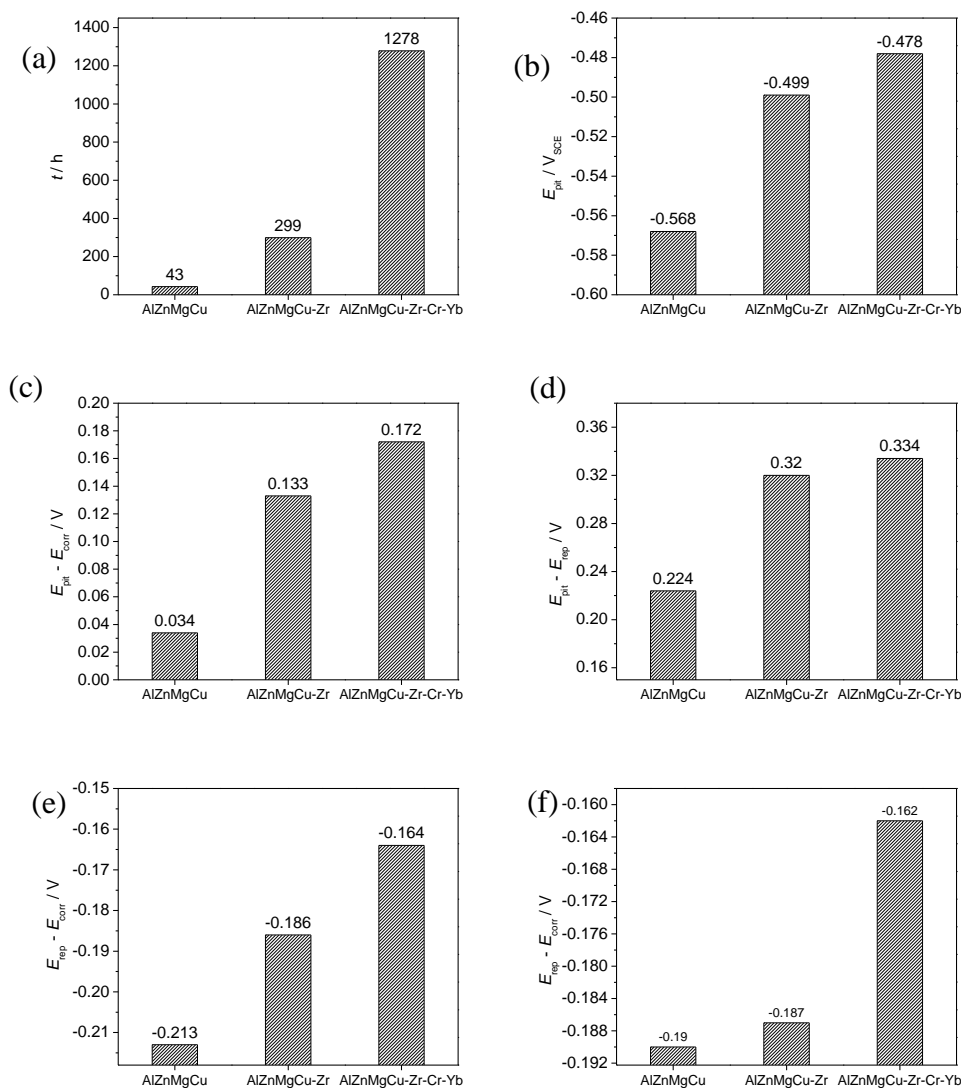

Figure 7. SCC initiation time (a), E_{pit} (b), E_{pit}–E_{corr} (c), E_{pit}–E_{rep} (d) , E_{rep}–E_{corr} in 3.5 wt% NaCl solution (e) and E_{rep}–E_{corr} in 0.1 mol/L Na_2SO_4 + 10 mmol/L NaCl solution (f) of the studied alloys

This can be explained from the perspective of corrosion mechanism of 7000 series Al alloys. Both SCC initiation time and these mentioned potential parameters are closely related with the initiation as well as the propagation of localized corrosion, especially the intergranular corrosion (IGC).

Potential differences (E_{pit}–E_{corr}, E_{pit}–E_{rep}, E_{corr}–E_{rep}) can be criteria to assess corrosion performance, especially for localized corrosion performance [30, 32, 34-37]. For instance, similar with E_{pit}, E_{pit}–E_{corr} can be used to evaluate the resistance of pitting initiation. The higher the difference between E_{pit} and E_{corr}, the harder pitting corrosion initiates [35]. As depicted in Fig. 8, the pits of 7150-T76 Al alloy (Al–6.5Zn–2.4Mg–2.2Cu–0.15Zr–0.08Fe) are both found in second phase and intergranular boundary. If the pits on intergranular boundary initiate, then further propagate along the boundary to some extent, the U-type specimens for SCC test would break down. Therefore, E_{pit} or E_{pit}–E_{corr}, related with the pitting initiation ability, shows the similar trend with SCC resistance, as shown in Fig. 7a-c.
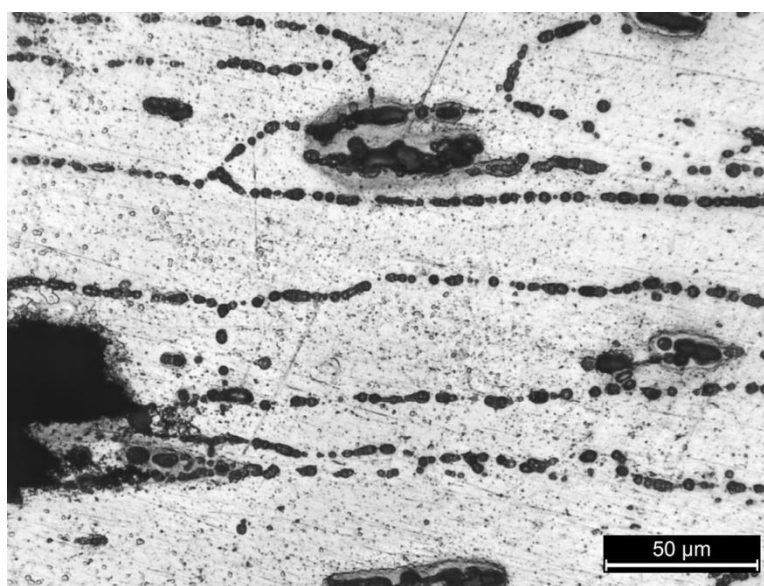

Figure 8. Corrosion morphology of 7150-T76 Al alloy (Al–6.5Zn–2.4Mg–2.2Cu–0.15Zr–0.08Fe) under chloride-containing solution

E_{pit}–E_{rep} has been used to determine the extent of crevice corrosion of steels [37] and to predict the propensity towards pitting of Al alloys [32], which was very effective. The upward trend of E_{pit}–E_{rep} shown in Fig. 7d indicates the addition of Zr, Cr and Yb impedes the propagation of localized corrosion. For a given condition, using E_{rep}–E_{corr} is effective to characterize the repassivation ability of an alloy [30]. In this condition, the upward trend of E_{rep}–E_{corr} shown in Fig. 7e (3.5 wt% NaCl) and Fig. 7f (0.1 mol/L Na_2SO_4 + 10 mmol/L NaCl) indicates improved repassivation ability is obtained by adding Zr, Cr and Yb to Al–6.2Zn–2.3Mg–2.3Cu alloy. In a word, both E_{pit}–E_{rep} and E_{rep}–E_{corr} are interrelated with the propagation of localized corrosion, mainly IGC, for 7000 series Al alloys. As a result, the alloys with micro-alloys show a prolonged cracking time. In addition, the excellent

agreement between SCC result and potential differences implies that electrochemical measurements can be an alternative to time-resuming SCC testing methods like U-type testing and double cantilever beam (DCB) testing when screening alloys or environments.

4.2 The Hall-Petch relation

As shown in Fig. 2, the mean grain size of these alloys is in the following order: AlZnMgCu > AlZnMgCu–Zr > AlZnMgCu–Zr–Cr–Yb. The difference of mean grain size is due to different recrystallization volume degree of these alloys. TEM micrographs of AlZnMgCu–Zr alloy and AlZnMgCu–Zr–Cr–Yb alloy are shown in Fig. 9. For AlZnMgCu–Zr alloy, due to the formation of Al_3Zr dispersoids [28], as can be seen in Fig. 9a, some of the subgrains growth are inhibited and therefore, reduce recrystallization volume degree. However, due to the relative unstable property of Al_3Zr, only part of deformation-recovery Al matrix microstructures was retarded [29], leading to a partially recrystallized microstructure. Whereas, as shown in Fig. 9b, complex addition of Zr, Cr and Yb can remarkably impede the recrystallization of Al matrix by forming 20–50 nm $(Zr,Yb)Cr_2(Al, Zr, Zn, Mg, Cu)_{20}$ dispersiods, which are more stable and finer than Al_3Zr dispersoids [15, 21, 23, 27-29]. Thus best grain refinement effect was obtained for Zr–Cr–Yb-containing alloy.
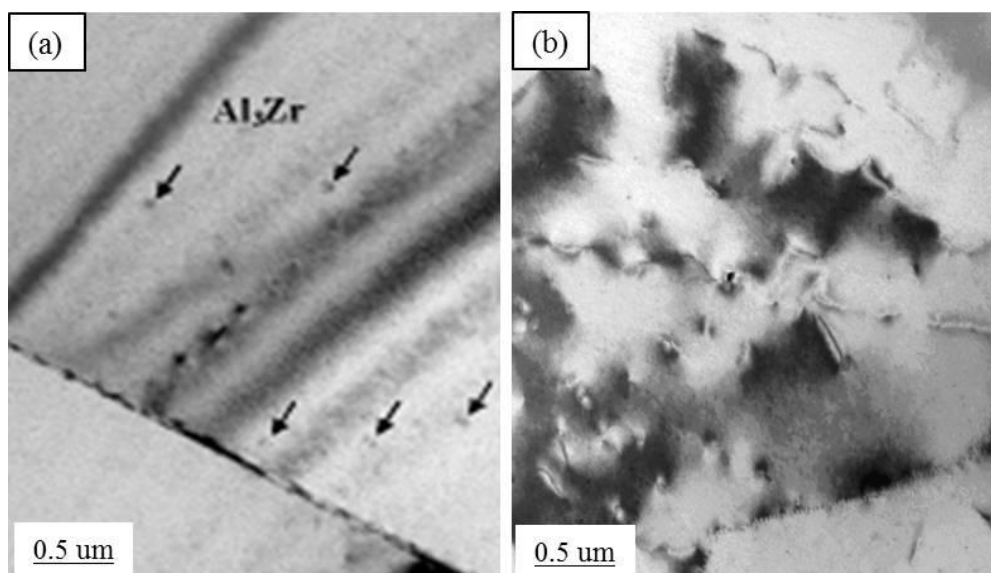

Figure 9. TEM micrographs of (a) AlZnMgCu–Zr alloy and (b) AlZnMgCu–Zr–Cr–Yb alloy

The Hall-Petch relation – strength is inversely proportional to grain size –has been validated by many researchers [38]. This work reconfirmed it. As shown in Fig. 9, the hardness of AlZnMgCu, AlZnMgCu–Zr and AlZnMgCu–Zr–Cr–Yb alloy is 173 Hv, 177 Hv and 184 Hv, respectively. Compared to base alloy, hardness increases for the Zr–containing alloy and the Zr–Cr–Yb–containing alloy. This is due to the formation of Al_3Zr (Zr–containing alloy) and $(Zr, Yb)Cr_2(Al, Zr, Zn, Mg, Cu)_{20}$ (Zr–Cr–Yb containing alloy) dispersoids which would lead to dispersoid strengthening, fine-grain strengthening, boundary strengthening and dislocation strengthening for Al–Zn–Mg–Cu alloys

[24, 25]. Better grain refinement effect was obtained by complex adding Zr, Cr and Yb than only adding Zr, which leads to further improvement of hardness property for Zr–Cr–Yb containing alloy.
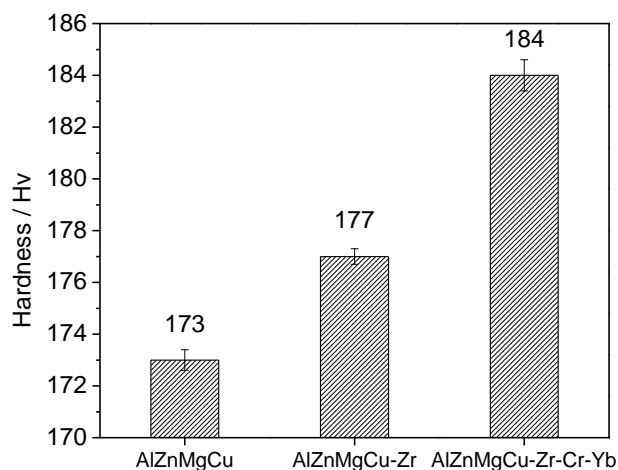

Figure 10. Hardness of T77 tempered alloys with different micro-alloys

Similar with strength property, corrosion resistance of alloys also can be related with grain size. The link between grain size and corrosion resistance has been reviewed and studied by N. Birbilis and his coworkers [9, 12, 13] who found that there is a tendency for corrosion rate to decrease as grain size decreases for high purity aluminium, and they further proposed that the Hall-Petch relation might exist between grain size and corrosion resistance. In the present work, the results reconfirmed their proposal. From SCC and electrochemical corrosion results, it can be concluded that the corrosion resistance of Al–6.2Zn–2.3Mg–2.3Cu alloys is inversely proportional to grain size. This is due to different low angle grain boundary (LAGB) densities of the studied alloys. Precious work revealed that in this three Al alloys, AlZnMgCu–Zr–Cr–Yb alloy has the highest proportion of LAGB [25, 27]. Since the energy of the LAGB is much lower than that of the HAGB and similar with grain interior energy, the concentration of η precipitates (anodic phase) at the LAGB is lower and the η phases are more discontinuously distributed [39, 40]. Grain boundaries with discrete η precipitates are noble to anodic dissolution and would cut off the corrosion channels for intergranular corrosion and SCC. Therefore, corrosion resistant of Al–6.2Zn–2.3Mg–2.3Cu alloys is improved by grain refinement which is caused by the addition of Zr or complex addition of Zr, Cr and Yb.

5. CONCLUSIONS

1) Compared to completely recrystallized AlZnMgCu alloy, AlZnMgCu–Zr alloy exhibits partially recrystallized microstructure due to the formation of Al$_3$Zr which would inhibit subgrains growth and recrystallization. Fibrous unrecrystallized microstructure with fine subgrains was obtained

for AlZnMgCu–Zr–Cr–Yb alloy due to the formation of $(Zr, Yb)Cr_2(Al, Zr, Zn, Mg, Cu)_{20}$ spherical dispersoids.

2) For Al–6.2Zn–2.3Mg–2.3Cu alloys, grain refinement by adding 0.16Zr and 0.16Zr–0.18Cr–0.3Yb leads to higher strength as well as better corrosion resistance, as revealed by hardness measurement, OCP, EIS and cyclic polarization tests. Particularly, SCC resistance is significantly improved by the complex addition of Zr, Cr and Yb, due to the completely inhibited recrystallization effect.

3) Grain size is determined by the recrystallization degree of Al alloys, which is related to micro-alloying additions. The hardness/strength of alloy enhances with the decline of grain size, which reconfirmed Hall-Petch relation. Similarly, Hall-Petch relation between corrosion resistance and grain size also was established.

4) Pitting potential and potential differences like $E_{pit}–E_{corr}$, $E_{pit}–E_{rep}$ and $E_{rep}–E_{corr}$ show the same trend with SCC initiation time. This is due to all these electrochemical parameters as well as SCC resistance are related with the initiation and propagation of pitting corrosion along the intergranular boundary.

Conflicts of interest:
The authors declare no conflict of interest.

References

1.   T. Dursun and C. Soutis, *Materials & Design*, 56 (2014) 862
2.   G. Peng, K. Chen, S. Chen and H. Fang, *Materials Science and Engineering: A*, 528 (2011) 4014
3.   Q. Meng and G. Frankel, *J. Electrochem. Soc.*, 151 (2004) B271
4.   Z. Szklarska-Smialowska, *Corros. Sci.*, 41 (1999) 1743
5.   T. Marlaud, B. Malki, C. Henon, A. Deschamps and B. Baroux, *Corros. Sci.*, 53 (2011) 3139
6.   Y. Reda, R. Abdel-Karim and I. Elmahallawi, *Materials Science and Engineering: A*, 485 (2008) 468
7.   A. Heinz, A. Haszler, C. Keidel, S. Moldenhauer, R. Benedictus and W. Miller, *Materials Science and Engineering: A*, 280 (2000) 102
8.   C. Feng, Z.-y. Liu, A.-l. Ning, Y.-b. Liu and S.-m. Zeng, *Transactions of Nonferrous Metals Society of China*, 16 (2006) 1163
9.   J. A. Wagner and R. Shenoy, *Metallurgical and Materials Transactions A*, 22 (1991) 2809
10.   J. Wloka and S. Virtanen, *Acta Mater.*, 55 (2007) 6666
11.   M. Mousavi and C. Cross, *Science and Technology of Welding & Joining*, 4 (1999) 381
12.   D. Xu, N. Birbilis and P. Rometsch, *Corros. Sci.*, 54 (2012) 17

13.   K. Ralston, N. Birbilis and C. Davies, *Scripta Mater.*, 63 (2010) 1201
14.   B. J. Ridder, A. Majumder and Z. K. Nagy, *Ind. Eng. Chem. Res.*, 53 (2014) 4387
15.   H. Fang, P. Shang, L. Huang, K. Chen, G. Liu and X. Xiong, *Mater. Lett.*, 75 (2012) 192
16.   K. Ralston and N. Birbilis, *Corrosion*, 66 (2010) 075005
17.   K. Ralston, D. Fabijanic and N. Birbilis, *Electrochim. Acta*, 56 (2011) 1729
18.   Y.-L. Wu, C. Li, F. S. Froes and A. Alvarez, *Metallurgical and Materials Transactions A*, 30 (1999) 1017
19.   D.-W. Suh, S.-Y. Lee, K.-H. Lee, S.-K. Lim and K. H. Oh, *J. Mater. Process. Technol.*, 155 (2004) 1330
20.   V. Davydov, T. Rostova, V. Zakharov, Y. A. Filatov and V. Yelagin, *Materials Science and Engineering: A*, 280 (2000) 30
21.   H. Fang, H. Chao and K. Chen, *J. Alloys Compd.*, 622 (2015) 166
22.   D. Xiao, J. Wang, D. Ding and H. Yang, *J. Alloys Compd.*, 352 (2003) 84
23.   G. Peng, K. Chen, H. Fang and S. Chen, *Materials & Design*, 36 (2012) 279
24.   H. Li, Z. Gao, H. Yin, H. Jiang, X. Su and J. Bin, *Scripta Mater.*, 68 (2013) 59
25.   H. Fang, K. Chen, X. Chen, H. Chao and G. Peng, *Corros. Sci.*, 51 (2009) 2872
26.   H. Fang, H. Chao and K. Chen, *Materials Science and Engineering: A*, 610 (2014) 10
27.   K. Chen, H.-C. Fang, Z. Zhang, X. Chen and G. Liu, *Materials Science and Engineering: A*, 497 (2008) 426
28.   Z. Zhang, K.-H. Chen, H.-C. Fang, X.-W. Qi and L. Gang, *Transactions of Nonferrous Metals Society of China*, 18 (2008) 1037
29.   G. Peng, K. Chen, H. Fang and S. Chen, *Materials Science and Engineering: A*, 535 (2012) 311
30.   D. Silverman, *Uhlig's Corrosion Handbook, Third Edition*, (2011) 1129
31.   R. Arrabal, B. Mingo, A. Pardo, M. Mohedano, E. Matykina and I. Rodríguez, *Corros. Sci.*, 73 (2013) 342
32.   M. Trueba and S. P. Trasatti, *Mater. Chem. Phys.*, 121 (2010) 523
33.   H. Ezuber, A. El-Houd and F. El-Shawesh, *Materials & Design*, 29 (2008) 801
34.   E. Rosen and D. Silverman, *Corrosion*, 48 (1992) 734
35.   W. Jiang, F. Jiang, B. Green, F. Liu, P. Liaw, H. Choo and K. Qiu, *Appl. Phys. Lett.*, 91 (2007) 041904
36.   D. C. Silverman, *Tutorial on cyclic potentiodynamic polarization technique*. 1998, NACE International, Houston, TX (United States).
37.   B. Wilde and E. Williams, *Electrochim. Acta*, 16 (1971)
38.   A. Chokshi, A. Rosen, J. Karch and H. Gleiter, *Scripta Metallurgica*, 23 (1989) 1679
39.   H. Tanaka, H. Esaki, K. Yamada, K. Shibue and H. Yoshida, *Materials Transactions*, 45 (2004) 69
40.   S. Kim, U. Erb, K. Aust and G. Palumbo, *Scripta Mater.*, 44 (2001) 835